Cloud Condensation Nuclei Activity of $CaCO_3$ Particles with Oleic Acid and Malonic Acid Coatings

Mingjin Wang[1,2], Tong Zhu[1*], Defeng Zhao[2], Florian Rubach[2,3], Andreas Wahner[2], Astrid Kiendler-Scharr[2], and Thomas F. Mentel[2*]

[1]BIC-ESAT and SKL-ESPCl, College of Environmental Sciences and Engineering, Peking University, Beijing 100871, China.

[2]Institut für Energie- and Klimaforschung (IEK-8), Forschungszentrum Jülich GmbH, 52425 Jülich, Germany.

[3]Klimageochemie, Max Planck Institut für Chemie, 55128 Mainz, Germany

[*] To whom correspondence should be addressed: tzhu@pku.edu.cn; t.mentel@fz-juelich.de

Abstract.

Condensation of carboxylic acids on mineral particles will lead to coatings, and impact on the particles' potential to act as cloud condensation nuclei (CCN). To determine how the CCN activity of mineral particles is impacted by carboxylic acid coatings, the CCN activities of $CaCO_3$ particles and $CaCO_3$ particles with oleic acid and malonic acid coatings were compared in this study. The results revealed that small

amounts of oleic acid coating (volume fraction (vf) ≤ 4.3%) decreased the CCN activity of $CaCO_3$ particles, while more oleic acid coating (vf ≥16%) increased the CCN activity of $CaCO_3$ particles. This phenomenon has not been reported before. On the other hand, the CCN activity of $CaCO_3$ particles coated with malonic acid increased with the thickness of the malonic acid coating (vf = 0.4 - 40%). Even smallest amounts of malonic acid coating (vf = 0.4%) significantly enhanced the CCN activity of $CaCO_3$ particles from $\kappa = 0.0028 \pm 0.0001$ to $\kappa = 0.0123 \pm 0.0005$. This supports that a small amount of water-soluble organic acid coating may significantly enhance the CCN activity of mineral particles. The presence of water vapor during the coating process with malonic acid additionally increased the CCN activity of the coated $CaCO_3$ particles, probably because more $CaCO_3$ reacts with malonic acid if sufficient water is available.

1 Introduction

Atmospheric aerosols serve as cloud condensation nuclei and change the radiative properties (cloud albedo effect) and lifetime (cloud lifetime effect) of clouds, thus affecting the Earth's climate indirectly (Liu and Wang, 2010; Gantt et al., 2012; Penner et al., 2004; Haywood and Boucher, 2000). Mineral aerosol is one of the most abundant components of the atmospheric aerosol. It is estimated that 1500-2600 Tg of mineral aerosol particles with radii between 0.1 and 8 μm are emitted annually into the atmosphere on a global scale (Cakmur et al., 2006). Mineral aerosol particles are mainly composed of substances that are slightly soluble or insoluble in water. Cloud condensation nuclei (CCN) activity measurements show that the hygroscopicity parameter κ (Petters and Kreidenweis, 2007) varies between 0.001 and 0.08 for mineral aerosols, including $CaCO_3$ aerosol, clay aerosols and mineral dust aerosols generated in the laboratory or sampled from various locations worldwide (Garimella et al., 2014; Yamashita et al., 2011; Zhao et al., 2010; Koehler et al., 2009; Sullivan et al., 2010; Herich et al., 2009). The low κ indicates that the CCN activity of mineral aerosol is much lower than that of water soluble salts like $(NH_4)_2SO_4$ (κ = 0.61) and NaCl (κ = 1.28), which are also common in atmospheric aerosols (Petters and Kreidenweis, 2007). Tang et al. (2016) reviewed recently the interaction of mineral dust particles with water.

Mineral aerosol particles can be coated by organic vapors during their residence and transport in the atmosphere. Many individual particle measurements have shown that mineral components and organic matter can coexist in the same individual aerosol

particle in the real atmosphere (Falkovich et al., 2004; Falkovich et al., 2001; Russell et al., 2002; Li and Shao, 2010). Carboxylic acids (R(C=O)OH) are abundant species among the organic matter that coexists with mineral particles. Russell et al. (2002) found that carbonyls (R(C=O)R), alkanes, and R(C=O)OH are present in individual mineral (and sea salt) aerosol particles, with enhanced concentration of R(C=O)OH. They also found that Ca^{2+}, CO_3^{2-}, R(C=O)OH and R(C=O)R coexisted in some individual mineral aerosol particles with a strong correlation between CO_3^{2-} and R(C=O)OH. These particles could be formed by $CaCO_3$ particles (partly) coated with organic film. Falkovich et al. (2004) also found that organic and inorganic components coexisted in individual mineral aerosol particles with the organic component consisting of various short-chain (C_1-C_{10}) mono- and dicarboxylic acids (MCA and DCA). The concentration of short-chain carboxylic acids in mineral aerosol particles increased with the increase of the ambient relative humidity. A possible explanation for such observations could be that when more water is condensed onto mineral particles at higher ambient relative humidity, the adsorbed carboxylic acids are ionized in the aqueous environment and react with mineral particles forming organic acid salts. Of the major components of mineral aerosol particles (clay, calcite ($CaCO_3$), quartz, mica, feldspar, etc.), only $CaCO_3$ with alkaline character can react with carboxylic acids in this way. Thus $CaCO_3$ may play a key role in the uptake of carboxylic acids by mineral aerosol particles.

Carboxylic acid coatings on mineral aerosol particles change their chemical composition and thus may have an impact on their CCN activity. Many previous studies have investigated the CCN activity of pure mineral aerosol (Garimella et al., 2014; Yamashita et al., 2011; Zhao et al., 2010; Koehler et al., 2009; Sullivan et al., 2010; Herich et al., 2009) and pure carboxylic acid aerosol (Kumar et al., 2003; Hori

et al., 2003; Cruz and Pandis, 1997; Hartz et al., 2006), but only a few studies have investigated the CCN activity of mineral aerosol particles with carboxylic acid coatings (Tang et al., 2015; Hatch et al., 2008; Gierlus et al., 2012).

In this study we used malonic acid and oleic acid as coating materials and $CaCO_3$ particles as cores, and investigated the CCN activity of the coated $CaCO_3$ particles. Herein we varied the coating thickness and the relative humidity during the coating process. Malonic acid is a representative of the class of dicarboxylic acids and oleic acid is an example of surfactant like compounds. Dicarboxylic acids are ubiquitous in the atmosphere (Kawamura et al., 1996; Kawamura and Ikushima, 1993; Ho et al., 2007; Mkoma and Kawamura, 2013; Kawamura and Bikkina, 2016) and formed by photochemical reactions and ozonolysis (Chebbi and Carlier 1996; Kawamura and Bikkina, 2016; Kawamura et al., 1996; Khare et al. 1999; Mellouki et al., 2015). It has been reported that dicarboxylic acids (C_2-C_{10}) account for 0.06-1.1% of the total aerosol mass, with higher values in the summer, and 1.8% of the total aerosol carbon (TC) in urban aerosol, in which oxalic acid, malonic acid, and succinic acid are the most abundant species (Kawamura et al., 1996; Kawamura and Ikushima, 1993; Ho et al., 2007; Mkoma and Kawamura, 2013). Oleic acid, which is emitted into the atmosphere by the cooking of meat, wood burning, and automobile source (Schauer et al., 1999; Rogge et al., 1998; Rogge et al., 1993), is present in atmospheric aerosols of urban, rural, and forest areas (Cheng et al., 2004; Ho et al., 2010). The water solubility of the two organic acids is complementary; it is high for malonic acid while it is very low for oleic acid. Coatings of malonic acid and oleic acid could thus have different effects on CCN activity of mineral particles.

2 Experimental

As general procedure, $CaCO_3$ aerosol was generated according to Zhao et al. (2010), and then poly- or monodisperse $CaCO_3$ aerosol particles were coated by malonic or oleic acid in a coating device. A flow tube was optionally applied to extend the residence time. The particle size, chemical composition, and CCN activity of the $CaCO_3$ particles were measured before and after coating. Figure 1 shows the schematic of the experimental set up.

2.1 Generation of $CaCO_3$ aerosol

$CaCO_3$ aerosol was generated by spraying a saturated $Ca(HCO_3)_2$ solution. A sample of $CaCO_3$ powder (2 g, pro analysis, ≥99%, Merck, Darmstadt, Germany) was suspended in 1-L Milli-Q water (18.2 MΩcm, TOC <5 ppb). Then about 1.5 L min^{-1} CO_2 (purity ≥99.995%, Praxair Industriegase GmbH & Co. KG, Magdeburg, Germany) was bubbled into the suspension at room temperature for 3 h, while the suspension was stirred using a magnetic stirrer. During bubbling, CO_2 reacted with $CaCO_3$ to produce $Ca(HCO_3)_2$. After bubbling, the suspension was allowed to settle for 10 min, the supernatant clear $Ca(HCO_3)_2$ solution was decanted and used for spraying by a constant output atomizer (Model 3076, TSI, Shoreview, MN, USA) using 1.75 L min^{-1} high-purity N_2 (Linde LiPur 6.0, purity 99.9999%, Linde AG, Munich, Germany).

125 The major portion (0.9 L min^{-1}) of the aerosol flow generated by spraying was dried
126 in a diffusion drier filled with silica gel. The relative humidity was below 10% after
127 drying. The remainder of the aerosol flow was drawn off by a pump and discarded.
128 The dry aerosol was passed through a tube furnace (Model RS 120/1000/12,
129 Nabertherm GmbH, Lilienthal, Germany) set at 300 ºC. The residence time of the
130 aerosol in the furnace was 5.2 s. Zhao et al. (2010) described this method for
131 generating $CaCO_3$ aerosol in detail. At room temperature dry $Ca(HCO_3)_2$ is
132 thermodynamically unstable and decays into $CaCO_3$, CO_2, and H_2O (Keiser and
133 Leavitt, 1908). With this method the aerosol still contained some $Ca(HCO_3)_2$ after
134 drying, but after heating at 300 ºC it was completely converted into $CaCO_3$ (Zhao et
135 al., 2010). The $CaCO_3$ aerosol generated was either first size selected by a Differential
136 Mobility Analyzer (DMA, TSI 3081) with a neutralizer on the inlet or entered the
137 coating device directly as poly-disperse aerosol.

138 Figure 2 (upper panel) shows the total number concentration and mean size of the
139 bare $CaCO_3$ aerosol particles generated at different spraying time, which were
140 measured with the SMPS described below. The mean size stabilized after about 50
141 min in the range 49.8-55.5 nm. Over the 232 min spraying time, the total number
142 concentration varied in the range $1.8 \cdot 10^6$–$4.5 \cdot 10^6$ cm^{-3}. The total number
143 concentration decreased by about 1/3 in the initial 70 min. The decrease became
144 slower after 70 min and the total number concentration tended to stabilize after 155
145 min. After 70 min the total number concentration varied in a smaller range of $1.8 \cdot 10^6$–
146 $2.9 \cdot 10^6$ cm^{-3}, therefore, the measurements in this study typically started after 70 min

147 spraying. The typical size distribution of the $CaCO_3$ aerosol particles after 70 min
148 spraying is shown in Fig. 2 (lower panel). The $CaCO_3$ particles showed a single mode
149 distribution with a mode diameter at 32.2 nm. The number concentration was more
150 than 10000 cm^{-3} for particles between 12.6 and 151.2 nm.

151 **2.2 Organic acid coating**

152 The coating device (Fig. 1, right hand side) used in this study was designed by Roselli
153 (2006), and showed good reproducibility, controllability, and stability. The glass
154 apparatus consisted of a small storage bulb (100 ml) holding the organic coating
155 substances which was directly connected to a mixing cell (about 35 ml). The storage
156 bulb and mixing cell were fully immersed in a flow-through water heater connected to
157 a thermostatic bath (F25, Julabo GmbH, Seelbach, Germany). The temperature range
158 of the thermostatic bath used in this study was 30-80 ºC. An extra N_2 stream could be
159 passed through the storage bulb in order to enhance the organic vapors flowing into
160 the mixing cell. The outflow of the coating device was connected to a Liebig type
161 water cooler. The water cooler was controlled by another thermostatic bath (F25,
162 Julabo GmbH, Seelbach, Germany) operated at 25 ºC throughout all of the
163 experiments.

164 The bottom of the storage bulb was filled with either 5.0 g malonic acid powder
165 (assay ≥98%(T), Fluka Chemika, Sigma-Aldrich, St Louis, MO, USA) or 10.0 ml
166 oleic acid (chemical purity (GC) 99.5%, Alfa Aesar, Ward Hill, MA, USA). A flow of
167 0.9 L min^{-1} high purity N_2 was used to carry the organic acid vapor up into the mixing
168 cell. The flow of 0.9 L min^{-1} $CaCO_3$ aerosol was passed through the mixing cell and
169 mixed with the 0.9 L min^{-1} N_2 flow carrying the organic acid vapor. The mixed flow

then entered the water cooler. The organic acid vapor was condensed on $CaCO_3$ aerosol particles in both the mixing cell and the water cooler. The residence time of the aerosol in the coating device including the cooler was about 6 seconds Three identical coating devices, with the same heating and cooling thermostatic bath, were used: one for malonic acid coating, one for oleic acid coating, and a blank one without organic acid for assessing the impact caused by heating the $CaCO_3$ aerosol in the coating device without organic acid (Roselli, 2006).

The aerosol could enter the measuring instruments directly, or after passing through a flow tube to increase its residence time. The flow tube was made of a straight circular glass tube with a 2.5 cm internal diameter. The aerosol flow in the flow tube was laminar flow. The average residence time of the aerosol in the flow tube was 23.7 s.

For the coating process we mixed flows of 0.9 L min^{-1} of dry N_2 and of aerosol dried to <10% relative humidity (RH) at room temperature (RT). As a consequence RH at the outlet of the coating device was <5% at RT. To investigate the impact of water on the coating process and CCN activity, organic coating at a higher relative humidity was also performed. For that a bubbling device filled with Milli-Q water was utilized to saturate the N_2 stream with water vapor before it entered the storage bulb (RH>90% at RT). After mixing with the aerosol stream at RH <10%, the water concentration in the mixing cell corresponded to RH ≈ 50% at RT or a partial pressure of ≈1500 Pa. The relative humidity of the aerosol at the outlet of the coating device at RT was indeed ~47% when humidification was applied. For the partial water vapor pressure of 1500 Pa we calculated RH >7% at 60°C (for MA), and RH >3% at 80°C (for OA) which is about an order of magnitude higher than RH in the dry cases. In fact RH will be somewhat higher as the gas-phase may not reach the bath temperature which

primarily serves to warm up the coating agent and control its vapor pressure.

2.3 Size and chemical composition measurements

The number size distribution of the aerosol particles was measured using a Scanning Mobility Particle Sizer (SMPS, TSI 3080 Electrostatic Classifier with TSI 3081 DMA, TSI 3786 UWCPC). The sample flow was set to 0.6 L min^{-1} and the sheath flow was set to 6.0 L min^{-1}. The size range measured was 9.82-414.2 nm with a size resolution of 64 channels per decade and the time resolution was 3 min for a complete scan. Despite the maximum resolution of the SMPS the size bin width was still substantial compared to the observed growth by coating. We therefore derived the diameter of the coated (and the respective bare $CaCO_3$ particles) by interpolating in between the size bins. For that we considered 5-9 size bins around the size bin of nominal mode and fitted a lognormal distribution to these data. The fitted mode positions are listed in Table 1. The error bars in x direction in Figure S1 in the supplement, show the shifts of the fitted mode position relative to the nominal size bin.

The chemical composition and the vacuum aerodynamic diameter of the aerosol particles were measured using a High-Resolution Time-of-Flight Aerosol Mass Spectrometer (HR-ToF-AMS, Aerodyne Research Inc., Billerica, MA, USA (DeCarlo et al., 2006)). The aerosol particles were vaporized at 600 ºC and ionized by electron impact ionization at 70 eV, i.e. we focused on the measurements of the organic coatings and sacrificed a direct $CaCO_3$ determination by AMS (compare Zhao et al. 2010). The AMS was routinely operated in V-mode in two alternating modes: 1 min MS mode to measure the chemical composition and 2 min PToF mode. Only MS mode data were analyzed. AMS measurements and SMPS measurements were synchronous and both were repeated at least four times for each sample. Size

information for bare $CaCO_3$ was taken from SMPS data in the blank coating device.

We used specific marker *m/z* to derive the amount of organic coating. For pure oleic acid the signal at *m/z*41 ($C_3H_5^+$) was reported to be the strongest signal in the mass spectrum measured by Q-AMS at EI energy of 70 eV and vaporizer temperature of 600 ºC (Sage et al., 2009). The signal at *m/z*41 was also strongest for oleic acid coatings in our HR mass spectra. In order to get a high signal to noise ratio we choose the signal at *m/z*41 in the MS mode of the AMS measurement as a marker for oleic acid in the coated $CaCO_3$ particles. There was no significant signal at *m/z*41 for the uncoated $CaCO_3$ particles. The average background signal at *m/z*41 per single aerosol particle corresponded to $2.7\pm0.9\cdot10^{-12}$ µg for bare $CaCO_3$. The average value presented the baseline of the mass spectra and the standard deviation was derived from the noise of the mass spectra at *m/z*41. Similarly, the signal at *m/z*42 ($C_2H_2O^+$) was one of the strongest signals in the mass spectrum of pure malonic particles measured by Q-AMS with EI energy of 70 eV and vaporizer temperature of 600 ºC (Takegawa et al., 2007). That signal was also observed for malonic acid coatings in our HR mass spectra and used as marker for malonic acid coatings. The average background signal per aerosol particle at *m/z42* for bare $CaCO_3$ particles was $1.4\pm0.4\cdot10^{-12}$µg. The average value represented the baseline of the mass spectra at *m/z*42 and the standard deviation was derived from the noise in the mass spectra.

The coating amount for both organic compounds was derived as follows. The observed signal at the respective marker *m/z* was corrected for the background signal from bare $CaCO_3$ and then scaled to the volume increase (per particle) calculated from the shift of the particle diameter D_P for the largest coating amount achieved at 80 ºC coating temperature. Because of the relative large bin width compared to the

growth by coating we used the D_P's, interpolated between the nominal size bins of the SMPS (see above). This assumed spherical core shell morphology, based on Zhao et al. (2011) where we showed that the $CaCO_3$ particles generated by our spray drying method are spherical. The relation between AMS derived organic mass (baseline corrected marker signals at *m/z41* or *m/z42* per particle) and SMPS derived organic mass ($\rho_{org} \times \pi/6 \times (D_P - D_{PCaCO3})^3$) is linear within the limits of the method (see Figure S1 in the supplement). For discussion we will refer to the AMS results, as we are able to detect amounts of organic coatings as small as few time 10^{-12} µg per particle with the AMS, while these could be not be detected by the SMPS.

2.4 CCN activity measurement

The aerosol was dried to RH <3% by another diffusion drier before the CCN activity was measured. To determine the CCN activity of the aerosol, the number concentration of the cloud condensation nuclei (CCN) of the aerosol was measured with a continuous flow CCN counter (CCNC, DMT-100, Droplet Measurement Technologies, Boulder, CO, USA). The total number concentration (CN) of the aerosol particles was synchronously measured using an ultrafine water-based condensation particle counter (UWCPC, TSI 3786, cf. Zhao et al., 2010). The ratio of CCN to CN (CCN/CN) is called the activated fraction (a_f). In cases where a poly-disperse aerosol was coated, the coated aerosol particles were size selected by scanning a DMA between 10.6 and 478.3 nm , and the CCN and CN concentrations were determined for each size bin while the supersaturation (SS) kept constant (known as 'Scanning Mobility CCN Analysis (SMCA)', Moore et al., 2010). The activated fraction was calculated after the CCN and CN concentrations were corrected for the multiple charged particles.

The activated fraction as a function of the particle size was fitted with a cumulative Gaussian distribution function (Rose et al., 2008). The turning point of the function is the critical dry diameter (D_{crit} or D_{50}) at the set SS. The activation efficiency (i.e., the activated fraction when aerosol particles are completely activated) was 83% for the CCN instrument, determined using 150 nm $(NH_4)_2SO_4$ particles at SS=0.85%. Besides $CaCO_3$ and coated $CaCO_3$ particles, the CCN activities of malonic acid particles, oleic acid particles, and mixed particles of $CaCO_3$ and malonic acid were also measured. The malonic acid particles were generated by spray-drying a malonic acid solution. The oleic acid particles were generated by heating 10.0 ml oleic acid to 97 ºC in the storage bulb and then cooling the vapor to 2 ºC in the water cooler in a clean coating device. 1.75 L min^{-1} high-purity N_2 was used as carrying gas and went into the storage bulb through‘1 N_2 in‘ entrance in Fig. 1; the‘3 Aerosol in‘ entrance in Fig. 1 was closed. This way, pure oleic acid particles with diameters up to 333 nm were generated. Mixed $CaCO_3$/malonic acid particles were generated by spraying the supernatant clear solutions which were prepared by settling suspensions containing $CaCO_3$ and malonic acid in molar ratios of about 1:1 and 3:1. The suspensions were prepared with 0.020 g malonic acid and 0.021 g $CaCO_3$ and 0.025 g malonic acid and 0.076 g $CaCO_3$ in 1000 ml Milli-Q water, respectively. The suspensions were allowed to stand for 24h.

For aerosols where monodisperse aerosol particles with a dry diameter D_P were coated, the CCN concentration was measured at different SS and the CN concentration was measured synchronously. Similarly, the activated fraction as a function of SS was fitted with a sigmoidal function. The turning point of the function is the critical supersaturation (SS_{crit}) and the corresponding dry diameter D_P is called the critical diameter, D_{crit}. The hygroscopicity parameter κ (Petters and Kreidenweis,

2007) was then calculated from the $D_P(D_{crit})$-SS_{crit} or $SS(SS_{crit})$-D_{crit} data set. The SS settings of the CCN counter were calibrated weekly using $(NH_4)_2SO_4$ aerosol based on the theoretic values in the literature (summarized by Rose et al., 2008).

3 Results and discussion

3.1 CCN activity of $CaCO_3$ aerosol

Before the coating experiments we determined the CCN activity of the bare $CaCO_3$ aerosol particles. It was measured by the SMCA method using poly-disperse $CaCO_3$ aerosol particles. The value of the hygroscopicity parameter κ of the $CaCO_3$ aerosol was 0.0028 ± 0.0001 derived by the least-square-fitting of D_{crit} as a function of SS (SS_{crit}). This κ value is quite small, indicating that the CCN activity of the $CaCO_3$ aerosol is low. Our κ is well within the range of κ's of 0.0011 ± 0.0004 to 0.0070 ± 0.0017 found in previous studies for wet generated $CaCO_3$ particles (Zhao et al., 2010; Sullivan et al., 2009; Gierlus et al., 2012, Tang et al., 2016), but larger than κ for dry generated $CaCO_3$ aerosols (0.0008-0.0018, Sullivan et al., 2009).

The CCN activity for $CaCO_3$ aerosol passed through the blank coating device exposed to temperatures of 60 ºC and 80 ºC was determined using the same method. The κ value remained at 0.0028 ± 0.0001 up to 60 ºC and increased to 0.0036 ± 0.0001 at 80 ºC. The increase in κ by 0.0008 at 80 ºC was smaller than the differences of reported κ values for $CaCO_3$ aerosol in various studies, and much smaller than the changes of κ values measured in this study when the $CaCO_3$ aerosol particles were coated by malonic or oleic acid. So the effect of heating the $CaCO_3$ aerosol during the coating

process on the CCN activity of the $CaCO_3$ aerosol was neglected. The D_{crit} at different supersaturations (SS_{crit}) for the $CaCO_3$ aerosol and for the $CaCO_3$ aerosol passed through a blank coating device at heating temperatures of 60 ºC and 80 ºC are shown in Fig. 5 (red, yellow and green circles).

As the solubility of $CaCO_3$ in water is very low, droplet activation of $CaCO_3$ (and other mineral dust components) is often described by a water adsorption approach, wherein the solute term B in the Köhler equation (Köhler 1936, Seinfeld and Pandis, 2006, see eq. (S1-S3) in the supplement) is replaced by a water adsorption term. The equations (1) and (2) show application of the Frenkel Halsey Hill adsorption isoterme (FHH) as proposed by Sorjamaa and Laaksonen (2007) and Kumar et al. (2009):

$$B = -A_{FHH} \cdot \theta^{-B_{FHH}} \quad (1)$$

Therein the water coverage θ (Sorjamaa and Laaksonen, 2007) is given as:

$$\theta = \frac{D_w - d_u}{2 \cdot 2.75 \cdot 10^{-4}} \quad [\mu m] \quad (2)$$

and D_w and d_u are the diameter of the wet particles and the insoluble core. We applied the FHH parameter for $CaCO_3$ (A_{FHH}=0.25 and B_{FHH}=1.19, Kumar et al. 2009) and derived a critical supersaturation of 1.52% for $CaCO_3$ particles with d_u = 101.9 nm (Figure 7, blue line). In comparison κ-Koehler theory predicts SS_{crit}=1.49% for κ=0.0028. Such an SS_{crit}=1.49% would also be achieved by $8.5 \cdot 10^{-20}$ mole solute per particle (Figure 7, black line). Figure 7 also shows the SS_{crit} for the bare $CaCO_3$ particles processed at 80 °C temperature and the range of SS_{crit} for 101.9 nm particles

calculated from the range of κ's given in the literature (Tang et al., 2016 and references therein) for wet generated $CaCO_3$ particles.

We conclude that the surface of our $CaCO_3$ particles is a little more wettable than the dry generated particles studied by Kumar et al. (2009). We presume formation of $Ca(OH)(HCO_3)$ structures on the surface during the spray-drying generation process as commonly observed whenever the $CaCO_3$ surface has been exposed to gaseous water or liquid water (Stipp, 1999; Stipp and Hochella, 1991; Neagle and Rochester, 1990). In case of soluble components cauisng the lower SS_{crit} their amount must be of the order of $1 \cdot 10^{-19}$ mole per particles.

3.2 CCN activity of $CaCO_3$ particles with oleic acid coating

For the coating with oleic acid, we selected monodisperse $CaCO_3$ aerosol particles of 101.8 nm diameter using the DMA, and measured the size and chemical composition of the particles before (uncoated) and after (coated) coating with oleic acid. The results are listed in the upper part of Table 1.

The mode diameters of number size distribution for the uncoated $CaCO_3$ particles at 30-80 ºC remained in the 101.8 nm size bin, identical to that selected by the DMA. Interpolation in between the size bins as described in the experimental section led to an average dry diameters of bare $CaCO_3$ of d_u = 101.9 nm. The mode diameters of the $CaCO_3$ particles after coating with oleic acid in the range of 30-50 ºC stayed in the pre-selected size bin at 101.8 nm, which means that the layers were too thin to

effectively grow the particles to the next size bin; the mode diameters increased distinctively in the temperature range of 60-80 ºC (Fig. 3, upper panel). However, the bin-interpolated diameters D_P which are shown in Table 1 increased monotonically over the whole temperature range.

The values of *m/z*41 [µg per particle] originating from the oleic acid coating for the coated $CaCO_3$ particles at 30-80 ºC were at all temperatures significantly larger than for the bare $CaCO_3$ particles, and increased with the increasing coating temperature ($3.7 \cdot 10^{-12}$ - $390 \cdot 10^{-12}$ µg per particle, compare Table 1 and Fig. 3, bottom panel, red circles). The AMS detected increase at *m/z41* showed that the $CaCO_3$ particles already contained small amounts of oleic acid after coating with oleic acid at temperatures below 60 ºC although the D_P shifted less than a size bin.

The organic volume fraction (vf) in the aerosol particles, V_{OA}/V_{par} [%], was calculated. Herein $V_{par} = (V_{OA} + V_{CaCO3})$, V_{OA} is the oleic acid volume derived by AMS and V_{CaCO3} the volume of the bare $CaCO_3$ before coating (101.9 nm). V_{OA}/V_{par} for the uncoated $CaCO_3$ particles is by definition zero. The vf for the coated $CaCO_3$ particles at 30-80 ºC increased with the increase in the coating temperature from 0.8% at 30 ºC to 44% at 80 ºC (Fig. 3, bottom panel, green square and Table 1). The $CaCO_3$ particles were indeed coated with a significant amount of oleic acid and the amount of oleic acid coating increased with the increase in the coating temperature. The experiments were repeated at least four times. The according standard deviations for the oleic acid mass per particle in Table 1 demonstrate that the reproducibility of the experiments

was good and the performance of the coating device was stable.

The activated fractions at different SS for monodisperse $CaCO_3$ particles with d_u = 101.9 nm before and after oleic acid coating at 30-80 ºC are shown in Fig. 4. The top panel in Fig. 4 shows the results at 30-60 ºC with up to $23\pm1.2\cdot10^{-12}$ μg of coating material deposited on the $CaCO_3$ particles (vf up to 4.3%). At the lowest SS of 0.17% and 0.35%, the activated fractions were very low and independent of the presence of the coating material within the errors. When the SS increased to 0.52%, 0.70%, and 0.87%, the activated fractions for the coated $CaCO_3$ particles were *lower* than those for the uncoated particles. Notably the activated fractions for the coated $CaCO_3$ particles *decreased* with the increase in the coating material in the range of vf 0.8-2.7%. The activated fractions for the $CaCO_3$ particles with different amounts of coating spread with larger SS applied. However this trend reversed at the coating temperature of 60 ºC and an oleic acid vf of 4.3%, and the activated fractions at vf = 4.3% became higher than those at 2.7% at the three largest SS. In summary, we found that the CCN activity of the coated $CaCO_3$ particles with vf of OA in a range 0.8-4.3% was lower than that of the uncoated $CaCO_3$ particles. The CCN activity of the coated $CaCO_3$ particles decreased with the increasing vf in between 0.8-2.7%, i.e. the CCN activity became lower when more coating material deposited on the $CaCO_3$ particles. This trend turned at a vf somewhere between 2.7 and 4.3%. As the D_P also increased at 60 ºC we cannot differentiate if the increase in the activated fractions is due to increasing size or because of increasing wettability.

394 The activated fractions of $CaCO_3$ particles after coating with oleic acid with vf of 16%
395 and 44% (coating temperatures of 70 and 80 ºC , respectively) were considerably
396 higher than that before coating, as shown in Fig. 4 (bottom panel). The increased
397 activated fractions resulted from both the increase in particle size (Fig. 3) and the
398 increase of the OA volume fraction of particles. At vf of 16% and 44%, the activated
399 fractions of the $CaCO_3$ particles after coating increased with the increase of SS and
400 reached complete activation. (Note, because the activation efficiency is 83%, the
401 activated fractions appear at values less than 100% at the points of full activation.)
402 For vf of 16% and 44% SS_{crit} was determined by fitting a sigmoidal function to the
403 activated fraction as a function of SS. The particle dry diameter D_P which is D_{crit} in
404 these cases is given in Table 1. The hygoscopicity parameter κ was determined from
405 D_P (D_{crit}) and the corresponding SS_{crit}. The κ values of the $CaCO_3$ particles coated
406 with vf of oleic acid of 16% and 44% were 0.0241±0.0006 and 0.0649±0.0008,
407 respectively. The respective κ values for the $CaCO_3$ particles with a diameter of 101.9
408 nm without coating and after coating with oleic acid at 30-60 ºC (oleic acid vf ≤4.3%)
409 could not be determined by this method because these particles could not be fully
410 activated at the highest SS reachable by the CCN counter. Therefore we give $\kappa =$
411 0.0028 ± 0.0001 for the uncoated $CaCO_3$ particles determined by scanning the size of
412 the poly-disperse $CaCO_3$ aerosol particles as described above (see Fig. 5).

413 So we conclude that for vf of oleic acid of 0.8-2.7% the CCN activity of $CaCO_3$
414 particles after coating is lower than that of uncoated $CaCO_3$ particles and decreases
415 with the fraction of oleic acid. The trend turns at a vf between 2.7 and 4.3%. CCN

activity was higher than that of the bare $CaCO_3$ particles at vf of oleic acid of 16% (70°C) and 44% (80°C) with CCN activity $\kappa = 0.0241 \pm 0.0006$ and $\kappa = 0.0649 \pm 0.0008$, respectively. The enhanced and reduced CCN activity of $CaCO_3$ particles coated with oleic acid at 80 ºC and 60 ºC, respectively, was also evident from the CCN activity measurement using *poly-disperse* aerosols (Fig. 5).

A possible explanation for our observation can be based on the amphiphilic character of oleic acid, namely that one end of the oleic acid molecule is hydrophobic (the hydrocarbon chain), while the other is hydrophilic (the carboxyl group).

We refer to $Ca(OH)(HCO_3)$ structures at the surface which offer polar surface sites to bind the hydrophilic ends (the carboxyl groups) of the oleic acid molecules. The hydrophobic ends of oleic acid molecules (the hydrocarbon chains) are then exposed on the particle surface hence increase the hydrophobicity of the particle surface. Such a formation of a hydrophobic layer should be occurring until all polar sites are occupied or monolayer coverage is reached, maybe in form of a self-assembled layer. This can hinder the uptake of water. Activation of $CaCO_3$ particles can be described by the Kelvin term and a water absorption term, e.g. Frenkel Halsey Hill isotherm (Sorjamaa and Laaksonen, 2007, Kumar et al., 2009). In terms of Kelvin/FHH theory the hydrophobic OA coating will lower A_{FHH} and/or likely increase B_{FHH}. The formation of a monolayer of OA on black carbon particles with the polar groups pointing outwards was postulated by Dalirian et al. (2017), which lead to increased activation of the black carbon particles. Thus, they observed a similar effect of layer

437 formation, but with switched polarity.

438 Garland et al. (2008) suggested that OA at sub-monolayer coverage form
439 self-associated islands rather than uniformly covering the surfaces, and OA molecules
440 are oriented vertically, with polar heads facing to the surface. This is in support of our
441 working hypothesis: the formation of a hydrophobic surface film. We conclude that
442 all hygroscopic sides on the $CaCO_3$ surface are covered at OA vf somewhere between
443 2.7% and 4.3%, as here the trend turns and droplet activation starts to increase again.
444 This would place the monolayer coverage above 3% organic volume fraction.
445 According to the measurements and calculations of the length of oleic acid molecule,
446 the thickness of oleic acid sub-monolayer on solid surfaces, and the thickness of
447 deuterated oleic acid monolayers at the air-water interface (Garland et al., 2008; King
448 et at., 2009; Iwahashi et al., 2000), we estimate 2.3 nm as the likely thickness of oleic
449 acid monolayer on $CaCO_3$ particles, accordingly a monolayer would be achieved at
450 about 12-13% organic volume fraction. As a consequence the re-increase of
451 hygroscopicity starts at sub-monolayer coverage and we propose that a fraction of
452 oleic acid binds to already adsorbed oleic acid tail by tail such that carboxylic groups
453 are facing outwards.

454 For $CaCO_3$ particles coated with more than an OA monolayer (vf = 16% and 44% at
455 70 and 80 ºC coating temperatures), OA in the first layer should still combine with the
456 $CaCO_3$ surface, the heads pointing downwards. We suppose that now a portion of the
457 carboxyl groups of the oleic acid molecules, which are not in the first layer, will be

458 exposed to the particle surface, in analogy to the formation of lipid bilayers, e.g. in
459 cells, though the structure of this part of oleic acid is not known. The particle surface
460 then becomes more hydrophilic.

461 When carboxylic groups of OA are exposed at the surface, the interaction of water
462 with the OA layer becomes stronger, and the surface becomes wettable. In terms of
463 the Kelvin/FHH approach, the surface water interaction becomes stronger and A_{FHH}
464 increases and likely also the interaction between the higher water layers (B_{FHH}
465 decreases). From this point of view water adsorption by the "OA bilayer" should
466 become similar to thin malonic acid layers (compare next section). In addition, when
467 droplets form, oleic acid will transfer to the surface of the droplets and lower the
468 surface tension of the solution (the surface tension of oleic acid is 0.033 J m^{-2}, which
469 is much lower than that of pure water of 0.072 J m^{-2}). Thus, the activation of OA
470 coated particles is probably a complex interaction between formation of a specific
471 hydrophobic layers and more hydrophilic multilayers, surface tension effects and for
472 the largest coating amounts, simple size effects. As shown in Figure 7, SS_{crit} for OA is
473 lower than for thin malonic acid coatings, probably because of the surface tension
474 effect, but higher than for thick MA coatings, because of the missing solute effect.

475 The CCN activity of all oleic coated particles is higher than the CCN activity of pure
476 oleic acid. Our CCN activity measurement showed that pure oleic acid particles up to
477 333 nm did not activate at 0.87% SS; this sets an upper limit for CCN activity of oleic
478 acid particles ($\kappa < 0.0005$), in agreement with Kumar et al. (2003) and Broekhuizen et

al. (2004). In liquid state oleic acid (OA) forms micelle like structures, the hydrophilic ends (the carboxyl groups) of oleic acid molecules tend to combine together by hydrogen bonds and the hydrophobic tails (the hydrocarbon chains) are exposed at the outside (Iwahashi et al., 2000; Garland et al., 2008). The arrangement of oleic acid molecules in pure oleic acid particles should be similar. Hydrophobic tails facing outwards can explain the hydrophobicity of the particle surface and the hindrance of the uptake of water, making the CCN activity of pure oleic acid particles very low. For sub-monolayer coatings of OA of vf 0.8 - 2.7% the CCN activity seem to approach that of pure OA. However, the arrangement of oleic acid molecules in these thin coatings will be influenced by the $CaCO_3$ core with its polar, hydrophilic sides differing from pure oleic acid particles and can thus be less hydrophobic.

Even at the largest coating with an organic volume fraction of 44%, the coating thickness is about 10 nm, which corresponds to about only 4 monolayers of oleic acid (assuming the thickness of oleic acid monolayer on $CaCO_3$ particles is about 2.3 nm). And the arrangement of oleic acid molecules will still be likely influenced by the $CaCO_3$ core. Water can probably adsorb at the carboxylic groups facing outward ("bilayer" type structure) and diffuse through the thin oleic acid coatings. It may form an adsorbed water phase near the $CaCO_3$ surface. This could push the oleic acid out to act as surfactant which lowers the Kelvin term. Such processes should also happen in pure oleic acid particles. Because of the presence of $CaCO_3$ core the SS to achieve this is lower than for pure OA.

500 The phenomenon described above is reported for the first time in the studies on the
501 CCN activity of multicomponent aerosols. This phenomenon also shows a limitation
502 of the otherwise very useful mixing rule (Petters and Kreidenweis, 2007) for
503 multicomponent aerosols with specific morphologies.

504 In Fig. 5 we additionally show the influence of water vapor on CCN activity of
505 $CaCO_3$ particles coated with oleic acid for the highest coating temperature (80 °C)
506 and thus largest oleic acid amount. Herein we determined D_{crit} at different
507 supersaturations (SS_{crit}) for *poly-disperse* $CaCO_3$ aerosol particles (by SMCA). The
508 experiments were performed at RH 0.3% and at RH 3% at the coating temperature of
509 80 °C on cooling to room temperature the RH increased to 47%. The presence of
510 more water vapor (1500 Pa) in the coating process increased κ somewhat and
511 enhanced the CCN activity. This is of importance since RH will often larger than 0.3%
512 if coating appears in the atmosphere. This will be discussed further in context of
513 malonic acid coatings at enhanced water vapor.

514 **3.3 CCN activity of $CaCO_3$ particles with malonic acid coating**

515 For the study with malonic acid coatings, the $CaCO_3$ particles were also size selected
516 with a diameter of 101.8 nm. The size D_P and chemical composition of $CaCO_3$ aerosol
517 particles are listed in Table 1 before and after coating with malonic acid (MA) at
518 temperatures in a range of 30-80 ºC. The mode diameter did not shift after coating in a
519 temperature range of 30-60 ºC, but it increased for coatings at 70 and 80 ºC with
520 increasing coating temperature. The size bin interpolated particle diameter D_P of the

521 MA coated particles increased monotonically with the coating temperature. The
522 average of the interpolated diameter of bare $CaCO_3$ particles in the temperature range
523 30°C-80°C was d_u = 101.9 nm.

524 Values of the malonic acid marker *m/z*42 per particle were significantly larger for
525 $CaCO_3$ particles after coating at 30-80 ºC and the MA mass increased from $3.3 \cdot 10^{-12}$
526 to $610 \cdot 10^{-12}$ µg per particle with the coating temperature (Table 1, Figure 3, bottom
527 panel). The organic volume fraction vf of malonic acid ($V_{MA}/(V_{MA}+V_{CaCO3})$[%]) was
528 calculated as in the case of the oleic acid and ranged from 0.4 to 40%. As for oleic
529 acid the malonic acid experiments were repeated at least four times and the
530 reproducibility and stability were good (see standard deviations in Table 1).

531 The activated fractions at different SS for 101.9 nm $CaCO_3$ particles before and after
532 coating with malonic acid at 30-80 ºC are shown in Fig. 6. SS_{crit} was determined by
533 fitting a sigmoidal function to the data and the κ value was calculated from the
534 $D_P(D_{crit})$ and the corresponding SS_{crit}. The results are listed in Table 1. In this
535 procedure we had to neglect the contribution of double charged particles as the step in
536 the CN/CCN vs SS data in Fig.6 is not sufficiently expressed to separate a plateau for
537 multiply charged particles (e.g. Sullivan et al., 2009). The exception is the MA
538 coating with vf = 0.4%. For this case we compared a sigmoidal fitting both from the
539 beginning (the first point) and from the multiply-charged plateau (the third point) to
540 the "completely-activated plateau" (Figure S3, supplement). We yield SS_{crit} =
541 0.887±0.005% for fitting from the beginning and SS_{crit} = 0.900±0.013% for fitting

from the multiply-charged plateau, a difference of 0.013%. The underestimate in SS_{crit} is the largest (0.013%) when the MA mass is the smallest (vf = 0.4%) and the underestimate will be reduced with increasing vf of MA. At the largest two MA vf it can be neglected. We have to concede a systematic error in SS_{crit}, but it is distinctively less than 0.02%.

The κ values of the $CaCO_3$ particles after coating with malonic acid at 30-80 ºC were higher than the κ value of the uncoated $CaCO_3$ particles (κ = 0.0028 ± 0.0001), and increased with the increasing coating MA mass per particle and increasing MA vf. The CCN activity of the $CaCO_3$ particles increased monotonically after coating with increasing malonic acid mass. This result differs from that of oleic acid which is not surprising since malonic acid is easily soluble in water.

The κ value for the $CaCO_3$ particles after coating with a mass of malonic acid as small as $3.3 \cdot 10^{-12}$ µg per particle and vf of MA of only 0.4% was 0.0123 ± 0.0005 thus considerably larger than the κ value for the uncoated $CaCO_3$ particles (κ = 0.0028 ± 0.0001). This suggests already that a small amount of malonic acid can significantly enhance the CCN activity of $CaCO_3$ particles. Such phenomenon, that traces of water soluble substances can strongly affect droplet activation has been reported before (Bilde and Svenningsson, 2004).

We applied Koehler theory to $CaCO_3$ particles coated with malonic acid assuming that the malonic acid coating will fully dissolve in water when droplets form (see supplement eq. (S1-S3). Increasing MA solute decreases the activity of water in

563 solution, and lowers the critical supersaturation SS_{crit} for droplet activation.

564 The resulting Koehler curves, i.e. equilibrium supersaturation (SS) over the solution
565 droplet as a function of the wet diameter D_w, are shown in Figure S2. Therein the
566 maximum of each SS curve is the critical supersaturation (theory SS_{crit}). In Table S1
567 and Figure 7 we compare the SS_{crit} predicted by the Köhler approach (red) with the
568 observed SS_{crit} (black). Koehler theory overpredicts SS_{crit} for thin coatings
569 substantially, meaning it underestimates the hygroscopicity of the thinly coated
570 particles. But with increasing coating Koehler theory approaches the observed SS_{crit}
571 and SS_{crit} for a particle of 121 nm diameter composed of pure malonic acid is the
572 limiting case (red circle).

573 From the Koehler results we derived the water content of the particles at SS_{crit} and we
574 calculated molality and mass fraction of the solute in the solution at the point of
575 activation. The molality at minimum and maximum malonic acid load of $3.3 \cdot 10^{-12}$
576 µg/particle and $610 \cdot 10^{-12}$ µg/particle were 0.006 mol kg^{-1} and 0.0015 mol kg^{-1},
577 respectively. We used these values in the AIOMFAC model (Zuend etal. 2011) to
578 calculate the deviation from ideality for the solution at point of activation for a flat
579 solution. The both solutions are highly non-ideal with respect to the MA (a_x = 0.4),
580 wherein MA was treated as solute with reference state infinite dilution (mole fraction
581 $x_{solute} \rightarrow 0$). However this did not affect much the activity coefficient of water, which
582 is essentially 1, water treated as solvent with reference state pure liquid (mole fraction
583 $x_{water} = 1$). Moreover, in this concentration range, the surface tension of aqueous

584 malonic acid solutions is about 0.070 J m^{-2}, thus the nearly same as for water (Table
585 S2 in the supplement). One should expect that Koehler theory would predict SS quite
586 well under such conditions.

587 To bring Köhler theory in agreement with the observation for the thinnest coating,
588 *more* solute entities would be required. Thus, disagreement cannot be caused by an ill
589 determined van't Hoff factor as we used already maximum $\nu = 3$ and reducing ν will
590 increase the deviation. Note, that recent observations point to the importance of the
591 surface effect by organic surface films over the solute effect for water soluble
592 inorganics in presence of organics, including malonic acid (Ruehl et al., 2016). A
593 lower surface tension will bring Koehler prediction and observation punctually in
594 better agreement and still allow for smaller van't Hoff factors (Varga et al., 2007). As
595 an example, a surface tension of 55% of σ_w and a van't Hoff factor of one will bring
596 SS_{crit} predicted by Koehler theory and observation in agreement for the thinnest
597 coating. However, a surface tension 55% of σ_w will cause disagreement for the
598 thickest coating, because the solute term gains in importance. Probably, the findings
599 for the mixed solutions of malonic acid and water soluble ammonium sulfate are not
600 directly transferable to our systems with insoluble inorganic core, where we expect
601 dilute aqueous solutions of 0.006 mol/kg of malonic acid at the activation point. At
602 such concentrations malonic acid does not reduce σ_w, moreover in the study of Ruehl
603 et al. (2016) malonic acid was one of the more Koehler κ behaving organics.

604 In Figure 7 we show the prediction of SS_{crit}=1.52% for activating $CaCO_3$ by the

605 Kelvin/FHH theory with the $CaCO_3$ parameters taken from Kumar et al. (2009). SS_{crit}
606 for our bare $CaCO_3$ particles is 1.49% and the lower SS_{crit} should be due to a more
607 adsorptive surface, e.g. the presence of $Ca(OH)(HCO_3)$ structures. According to
608 classical Koehler theory the equivalent of $8.5 \cdot 10^{-20}$ moles of dissolvable entities
609 would be needed to explain a κ of 0.0028 and SS_{crit} of 1.49%, which is only about ¼
610 of the moles MA in the thinnest MA coating. Therefore, whatever makes our $CaCO_3$
611 particles wettable is not sufficient to explain the low SS_{crit} of 0.9 % at the thinnest MA
612 coating in terms of Koehler theory.

613 We estimate monolayer coverage by MA at 2-3% vf; this would be achieved in
614 between MA mass loads of $13 \cdot 10^{-12}$ - $38 \cdot 10^{-12}$ µg per particle. Thus a sub-monolayer
615 coating of $3.3 \cdot 10^{-12}$ µg MA per particle caused a drop of SS_{crit} from 1.49 to 0.9 and
616 increased κ from 0.0028 to 0.012. Therefore we conclude that $CaCO_3$/MA coatings
617 show a non-Koehler behavior at thin coatings, but approach Koehler behavior with
618 increasing MA load.

619 This means there must be specific interactions between MA and the $CaCO_3$ surface
620 which eases water adsorption and CCN activation. We refer to the $Ca(OH)(HCO_3)$
621 structures that likely exist on the particle surface. When $CaCO_3$ particles are coated by
622 malonic acid (or oleic acid) the hydrophilic sides can serve as polar surface active
623 sites for accommodation of the acids. In case of MA there is no long hydrophobic
624 organic chain, but a second carboxylic group which still could support the adsorption
625 of water films.

In terms of Kelvin/FHH theory one could explain the observed low SS_{crit} for thin MA coatings by net stronger interaction with water (higher A_{FHH}) and/or stronger interaction between the adsorbed water layers (lower B_{FHH}) compared to bare $CaCO_3$. If coatings become thicker the Koehler solute effect starts increasingly to contribute and eventually controls the CCN activation. Our data are not sufficient to determine A_{FHH} and B_{FHH}. (The only system in the literature which comes close - in a far sense - is CaOxalate Monohydrate, with $A_{FHH} = 0.57$ of and $B_{FHH} = 0.88$ (Kumar et al., 2009). Plugin in these FHH parameters will lead to $SS_{crit} = 0.53\%$ commensurable with our observed value of 0.56% for $13 \cdot 10^{-12}$ µg MA coating which represents an organic volume fraction of 1.5%, thus is close to monolayer.)

The D_{crit} at different supersaturations (SS_{crit}) for *poly-disperse* $CaCO_3$ aerosol particles before and after coating with malonic acid are shown in Fig. 8. Our observation of $\kappa = 0.25 \pm 0.04$ for pure malonic is consistent with the κ derived from the data of Kumar et al. (2003) ($\kappa = 0.20$-0.25) and Prenni et al. (2001) ($\kappa = 0.24$), but significantly lower than the κ derived from the data of Giebl et al. (2002) ($\kappa =$ 0.41-1.04). The behavior of poly-disperse coated aerosol was similar to the result obtained from the monodisperse $CaCO_3$ aerosol particles.

In Fig. 8 we added results for coating in presence of enhanced water vapor (1500 Pa) and aerosols generated by spraying mixtures of malonic acid and $CaCO_3$. At the coating temperature of 60 ºC, when the RH increased from 0.7% to 7% and eventually to 47% at room temperature, the CCN activity of the coated $CaCO_3$ particles

increased substantially (compare "dry" (green triangles) and "wet" (lilac triangles) in Fig. 8). The effect is more distinct than for the oleic acid coating shown in Fig. 5, and κ increases by about an order of magnitude. At a wet conditions, the reaction between $CaCO_3$ and malonic acid maybe more efficient and formation of calcium malonate will reduce d_u, i.e. the diameter of the insoluble core and according to eq, (S1) this may be the reason for the higher CCN activity at the higher RH. The hypothesis of malonate formation is supported by the CCN activity of "calcium malonate" aerosols, generated by spraying solutions containing $CaCO_3$ and malonic acid with molar ratios of about 1:1 and 3:1. Here the CCN activity is similar to that arising in the coating process in presence of water vapor. The change of the Ca/malonate ratio from 3:1 to 1:1 had no large effects. But taking the data of pure malonic acid particles also into account there is a trend to lower κ with increasing Ca in the initial solution.

The increasing of residence time (by 23.7 s) had no significant impact on CCN activity for both oleic acid coating and malonic acid coating at both dry and enhanced water vapor conditions, probably because the coating process was already completed in the coating device and no further reactions occurred in the flow tube.

Our findings may be important for aging processes of mineral particles in the atmosphere. The dependence of CCN activity of the coated particles on RH during the coating process will help to enhance the increase of the CCN activity by the coating process as water will be abundant in many instances. The effect probably will be relatively small for oleic acid and similar organics, which are hardly water soluble,

668 but strong for malonic acid and similar organic acids, which are highly water soluble.

669 ## 4 Conclusions

670 The CCN activity of $CaCO_3$ particles with oleic acid and malonic acid coatings was
671 investigated in this study. The results show that oleic acid coating and malonic acid
672 coating have different impacts on the CCN activity of $CaCO_3$ particles. This can be
673 attributed to the amphiphilic property of oleic acid in contrast to the high water
674 solubility of malonic acid. Small amounts of oleic acid coating ($vf \leq 4.3\%$) decreased
675 the CCN activity of the $CaCO_3$ particles, while more oleic acid coating ($vf \geq 16\%$)
676 increased it. This phenomenon was reported here for the first time, and attributed to
677 stepwise passivating the active sites of $CaCO_3$ by oleic acid. Once all active sites are
678 occupied we suggest the formation of a lipid like bilayer with the carboxylic groups
679 facing outwards.

680 On the other hand, malonic acid coating (0.4-40%) increased the CCN activity of
681 $CaCO_3$ particles regardless of the amount of the coating. The CCN activity of $CaCO_3$
682 particles with malonic acid coating increased with the amount of the coating. Even a
683 small amount of malonic acid coating ($vf = 0.4\%$) significantly enhanced the CCN
684 activity of $CaCO_3$ particles from $\kappa = 0.0028 \pm 0.0001$ to $\kappa = 0.0123 \pm 0.0005$.
685 Increasing the relative humidity during the coating increased the CCN activity of the
686 $CaCO_3$ particles with malonic acid coating, probably because more $CaCO_3$ reacted
687 with malonic acid to soluble CaMalonate. This process will help to increase the CCN
688 activity.

Although malonic acid is well soluble in water, SS_{crit} for MA coated particles was overpredicted by Köhler theory. Our results indicate that thin MA coatings provide a wettable particle surface, which favors adsorption of water. For thicker coatings the coated particles approached Köhler behavior, because of increasing importance of the solute effect.

Mineral aerosol is one of the most abundant components of the atmospheric aerosol, but its low water solubility limits its CCN activity. This study showed that water-soluble organic acid coating might significantly enhance the CCN activity of mineral aerosol particles. This could lead to mineral aerosol playing a more important role in cloud formation.

Acknowledgments

This study was supported by Forschungszentrum Jülich, the National Natural Science Foundation Committee of China (41421064, 21190051, 41121004), and the China Scholarship Council.

706 **References**

707 AIOMFAC model, http://www.aiomfac.caltech.edu

708 Broekhuizen, K. E., Thornberry, T., Kumar, P. P., and Abbatt, J. P. D.: Formation of cloud
709 condensation nuclei by oxidative processing: Unsaturated fatty acids, J. Geophys.
710 Res.-Atmos., 109, D24206, 10.1029/2004jd005298, 2004.

711 Cakmur, R. V., Miller, R. L., Perlwitz, J., Geogdzhayev, I. V., Ginoux, P., Koch, D., Kohfeld,
712 K. E., Tegen, I., and Zender, C. S.: Constraining the magnitude of the global dust cycle by
713 minimizing the difference between a model and observations, J. Geophys. Res.-Atmos., 111,
714 D06207, 10.1029/2005jd005791, 2006.

715 Charbouillot, T., Gorini, S., Voyard, G., Parazols, M., Brigante, M., Deguillaume, L., Delort,
716 A. M., and Mailhot, G.: Mechanism of carboxylic acid photooxidation in atmospheric
717 aqueous phase: Formation, fate and reactivity, Atmos. Environ., 56, 1-8,
718 10.1016/j.atmosenv.2012.03.079, 2012.

719 Chebbi, A. and P. Carlier (1996). "Carboxylic acids in the troposphere, occurrence, sources,
720 and sinks: A review." Atmospheric Environment 30(24): 4233-4249.

721 Cheng, Y., Li, S. M., Leithead, A., Brickell, P. C., and Leaitch, W. R.: Characterizations of
722 cis-pinonic acid and n-fatty acids on fine aerosols in the Lower Fraser Valley during Pacific
723 2001 Air Quality Study, Atmos. Environ., 38, 5789-5800, 10.1016/j.atmosenv.2004.01.051,
724 2004.

725 Chumpitaz, L. D. A., Coutinho, L. F., and Meirelles, A. J. A.: Surface tension of fatty acids
726 and triglycerides, J. Am. Oil Chem. Soc., 76, 379-382, 10.1007/s11746-999-0245-6, 1999.

727 Cruz, C. N., and Pandis, S. N.: A study of the ability of pure secondary organic aerosol to act
728 as cloud condensation nuclei, Atmos. Environ., 31, 2205-2214,
729 10.1016/s1352-2310(97)00054-x, 1997.

730 Dalirian, M., Ylisirniö, A., Buchholz, A., Schlesinger, D., Ström, J., Virtanen, A., and
731 Riipinen, I.: Cloud droplet activation of black carbon particles coated with organic
732 compounds of varying solubility, Atmos. Chem. Phys. Discuss., 2017, 1-25,
733 10.5194/acp-2017-1084, 2017.

734 DeCarlo, P. F., Kimmel, J. R., Trimborn, A., Northway, M. J., Jayne, J. T., Aiken, A. C.,
735 Gonin, M., Fuhrer, K., Horvath, T., Docherty, K. S., Worsnop, D. R., and Jimenez, J. L.:
736 Field-deployable, high-resolution, time-of-flight aerosol mass spectrometer, Anal. Chem., 78,
737 8281-8289, 10.1021/ac061249n, 2006.

738 Falkovich, A. H., Ganor, E., Levin, Z., Formenti, P., and Rudich, Y.: Chemical and
739 mineralogical analysis of individual mineral dust particles, J. Geophys. Res.-Atmos., 106,
740 18029-18036, 10.1029/2000jd900430, 2001.

741 Falkovich, A. H., Schkolnik, G., Ganor, E., and Rudich, Y.: Adsorption of organic
742 compounds pertinent to urban environments onto mineral dust particles, J. Geophys.
743 Res.-Atmos., 109, D02208, 10.1029/2003jd003919, 2004.

744 Gantt, B., Xu, J., Meskhidze, N., Zhang, Y., Nenes, A., Ghan, S. J., Liu, X., Easter, R., and
745 Zaveri, R.: Global distribution and climate forcing of marine organic aerosol - Part 2: Effects
746 on cloud properties and radiative forcing, Atmos. Chem. Phys., 12, 6555-6563,
747 10.5194/acp-12-6555-2012, 2012.

748 Garimella, S., Huang, Y. W., Seewald, J. S., and Cziczo, D. J.: Cloud condensation nucleus
749 activity comparison of dry- and wet-generated mineral dust aerosol: the significance of
750 soluble material, Atmos. Chem. Phys., 14, 6003-6019, 10.5194/acp-14-6003-2014, 2014.

751 Garland, E. R., Rosen, E. P., Clarke, L. I., and Baer, T.: Structure of submonolayer oleic acid
752 coverages on inorganic aerosol particles: evidence of island formation, Phys. Chem. Chem.
753 Phys., 10, 3156-3161, 10.1039/b718013f, 2008.

754 Giebl, H., Berner, A., Reischl, G., Puxbaum, H., Kasper-Giebl, A., and Hitzenberger, R.:
755 CCN activation of oxalic and malonic acid test aerosols with the University of Vienna cloud
756 condensation nuclei counter, J. Aerosol Sci., 33, 1623-1634, Pii s0021-8502(02)00115-5,
757 10.1016/s0021-8502(02)00115-5, 2002.

758 Gierlus, K. M., Laskina, O., Abernathy, T. L., and Grassian, V. H.: Laboratory study of the
759 effect of oxalic acid on the cloud condensation nuclei activity of mineral dust aerosol, Atmos.
760 Environ., 46, 125-130, 10.1016/j.atmosenv.2011.10.027, 2012.

761 Hartz, K. E. H., Tischuk, J. E., Chan, M. N., Chan, C. K., Donahue, N. M., and Pandis, S. N.:
762 Cloud condensation nuclei activation of limited solubility organic aerosol, Atmos. Environ.,
763 40, 605-617, 10.1016/j.atmosenv.2005.09.076, 2006.

764 Hatch, C. D., Gierlus, K. M., Schuttlefield, J. D., and Grassian, V. H.: Water adsorption and
765 cloud condensation nuclei activity of calcite and calcite coated with model humic and fulvic
766 acids, Atmos. Environ., 42, 5672-5684, 10.1016/j.atmosenv.2008.03.005, 2008.

767 Haywood, J., and Boucher, O.: Estimates of the direct and indirect radiative forcing due to
768 tropospheric aerosols: A review, Reviews of Geophysics, 38, 513-543,
769 10.1029/1999rg000078, 2000.

770 Herich, H., Tritscher, T., Wiacek, A., Gysel, M., Weingartner, E., Lohmann, U.,
771 Baltensperger, U., and Cziczo, D. J.: Water uptake of clay and desert dust aerosol particles at
772 sub- and supersaturated water vapor conditions, Phys. Chem. Chem. Phys., 11, 7804-7809,
773 10.1039/b901585j, 2009.

774 Ho, K. F., Cao, J. J., Lee, S. C., Kawamura, K., Zhang, R. J., Chow, J. C., and Watson, J. G.:
775 Dicarboxylic acids, ketocarboxylic acids, and dicarbonyls in the urban atmosphere of China,
776 J. Geophys. Res.-Atmos., 112, D22s27, 10.1029/2006jd008011, 2007.

777 Ho, K. F., Lee, S. C., Ho, S. S. H., Kawamura, K., Tachibana, E., Cheng, Y., and Zhu, T.:
778 Dicarboxylic acids, ketocarboxylic acids, alpha-dicarbonyls, fatty acids, and benzoic acid in
779 urban aerosols collected during the 2006 Campaign of Air Quality Research in Beijing
780 (CAREBeijing-2006), J. Geophys. Res.-Atmos., 115, D19312, 10.1029/2009jd013304, 2010.

781 Hori, M., Ohta, S., Murao, N., and Yamagata, S.: Activation capability of water soluble
782 organic substances as CCN, J. Aerosol Sci., 34, 419-448, 10.1016/s0021-8502(02)00190-8,

2003.

Iwahashi, M., Kasahara, Y., Matsuzawa, H., Yagi, K., Nomura, K., Terauchi, H., Ozaki, Y., and Suzuki, M.: Self-diffusion, dynamical molecular conformation, and liquid structures of n-saturated and unsaturated fatty acids, J. Phys. Chem. B, 104, 6186-6194, 10.1021/jp000610l, 2000.

Kawamura, K., and Ikushima, K.: Seasonal-changes in the distribution of dicarboxylic-acids in the urban atmosphere, Environ. Sci. Technol., 27, 2227-2235, 10.1021/es00047a033, 1993.

Kawamura, K., Kasukabe, H., and Barrie, L. A.: Source and reaction pathways of dicarboxylic acids, ketoacids and dicarbonyls in arctic aerosols: One year of observations, Atmos. Environ., 30, 1709-1722, 10.1016/1352-2310(95)00395-9, 1996.

Kawamura, K., and Bikkina, S.: A review of dicarboxylic acids and related compounds in atmospheric aerosols: Molecular distributions, sources and transformation, Atmospheric Research, 170, 140-160, 10.1016/j.atmosres.2015.11.018, 2016.

Keiser, E. H., and Leavitt, S.: On the preparation and the composition of the acid carbonates of calcium and barium, J. Am. Chem. Soc. , 30, 1711-1714, 10.1021/ja01953a008, 1908.

Khare, P., et al. (1999). "Atmospheric formic and acetic acids: An overview." Reviews of Geophysics 37(2): 227-248.

King, M. D., Rennie, A. R., Thompson, K. C., Fisher, F. N., Dong, C. C., Thomas, R. K., Pfrang, C., and Hughes, A. V.: Oxidation of oleic acid at the air-water interface and its potential effects on cloud critical supersaturations, Phys. Chem. Chem. Phys., 11, 7699-7707, 10.1039/b906517b, 2009.

Koehler, H.: The nucleus in and the growth of hygroscopic droplets, Trans. Faraday Soc., 32, 1152-1161, 10.1039/tf9363201152, 1936.

Koehler, K. A., Kreidenweis, S. M., DeMott, P. J., Petters, M. D., Prenni, A. J., and Carrico, C. M.: Hygroscopicity and cloud droplet activation of mineral dust aerosol, Geophys. Res. Lett., 36, L08805, 10.1029/2009gl037348, 2009.

Kumar, P. P., Broekhuizen, K., and Abbatt, J. P. D.: Organic acids as cloud condensation nuclei: Laboratory studies of highly soluble and insoluble species, Atmos. Chem. Phys., 3, 509-520, 2003.

Kumar, P., Nenes, A., and Sokolik, I. N.: Importance of adsorption for CCN activity and hygroscopic properties of mineral dust aerosol, Geophys. Res. Lett., 36, 10.1029/2009gl040827, 2009.

Li, W. J., and Shao, L. Y.: Mixing and water-soluble characteristics of particulate organic compounds in individual urban aerosol particles, J. Geophys. Res.-Atmos., 115, D02301, 10.1029/2009jd012575, 2010.

Liu, X. H., and Wang, J. A.: How important is organic aerosol hygroscopicity to aerosol indirect forcing?, Environ. Res. Lett., 5, 044010, 10.1088/1748-9326/5/4/044010, 2010.

Mkoma, S. L., and Kawamura, K.: Molecular composition of dicarboxylic acids, ketocarboxylic acids, alpha-dicarbonyls and fatty acids in atmospheric aerosols from Tanzania, East Africa during wet and dry seasons, Atmos. Chem. Phys., 13, 2235-2251, 10.5194/acp-13-2235-2013, 2013.

Moore, R. H., Nenes, A., and Medina, J.: Scanning Mobility CCN Analysis-A Method for Fast Measurements of Size-Resolved CCN Distributions and Activation Kinetics, Aerosol Sci. Technol., 44, 861-871, 10.1080/02786826.2010.498715, 2010.

Neagle, W., and Rochester, C. H., Infrared study of the adsorption of water and ammonia on calcium carbonate. Journal of the Chemical Society, Faraday Transactions, 86, 181-183, 1990.

Penner, J. E., Dong, X. Q., and Chen, Y.: Observational evidence of a change in radiative forcing due to the indirect aerosol effect, Nature, 427, 231-234, 10.1038/nature02234, 2004.

Petters, M. D., and Kreidenweis, S. M.: A single parameter representation of hygroscopic growth and cloud condensation nucleus activity, Atmos. Chem. Phys., 7, 1961-1971, 2007.

Rogge, W. F., Hildemann, L. M., Mazurek, M. A., Cass, G. R., and Simoneit, B. R. T.: Sources of fine organic aerosol .2. Noncatalyst and catalyst-equipped automobiles and heavy-duty diesel trucks, Environ. Sci. Technol., 27, 636-651, 10.1021/es00041a007, 1993.

Rogge, W. F., Hildemann, L. M., Mazurek, M. A., Cass, G. R., and Simoneit, B. R. T.: Sources of fine organic aerosol. 9. Pine, oak and synthetic log combustion in residential fireplaces, Environ. Sci. Technol., 32, 13-22, 10.1021/es960930b, 1998.

Rose, D., Gunthe, S. S., Mikhailov, E., Frank, G. P., Dusek, U., Andreae, M. O., and Poschl, U.: Calibration and measurement uncertainties of a continuous-flow cloud condensation nuclei counter (DMT-CCNC): CCN activation of ammonium sulfate and sodium chloride aerosol particles in theory and experiment, Atmos. Chem. Phys., 8, 1153-1179, 2008.

Ruehl, C. R., Davies, J. F., and Wilson, K. R.: An interfacial mechanism for cloud droplet formation on organic aerosols, Science, 351, 1447-1450, 10.1126/science.aad4889, 2016.

Russell, L. M., Maria, S. F., and Myneni, S. C. B.: Mapping organic coatings on atmospheric particles, Geophys. Res. Lett., 29, 1779, 10.1029/2002gl014874, 2002.

Sage, A. M., Weitkamp, E. A., Robinson, A. L., and Donahue, N. M.: Reactivity of oleic acid in organic particles: changes in oxidant uptake and reaction stoichiometry with particle oxidation, Phys. Chem. Chem. Phys., 11, 7951-7962, 10.1039/b904285g, 2009.

Schauer, J. J., Kleeman, M. J., Cass, G. R., and Simoneit, B. R. T.: Measurement of emissions from air pollution sources. 1. C-1 through C-29 organic compounds from meat charbroiling, Environ. Sci. Technol., 33, 1566-1577, 10.1021/es980076j, 1999.

Sorjamaa, R., and Laaksonen, A.: The effect of H_2O adsorption on cloud drop activation of insoluble particles: a theoretical framework, Atmos. Chem. Phys., 7, 6175-6180, 10.5194/acp-7-6175-2007, 2007.

Stipp, S. L. S.: Toward a conceptual model of the calcite surface: hydration, hydrolysis, and

surface potential. Geochimica et Cosmochimica Acta, 63, 3121-3131, 1999.

Stipp, S. L., Hochella Jr, M. F.: Structure and bonding environments at the calcite surface as observed with X-ray photoelectron spectroscopy (XPS) and low energy electron diffraction (LEED). Geochimica et Cosmochimica Acta, 55, 1723-1736,1991.

Sullivan, R. C., Moore, M. J. K., Petters, M. D., Kreidenweis, S. M., Roberts, G. C., and Prather, K. A.: Effect of chemical mixing state on the hygroscopicity and cloud nucleation properties of calcium mineral dust particles, Atmos. Chem. Phys., 9, 3303-3316, 10.5194/acp-9-3303-2009, 2009.

Sullivan, R. C., Moore, M. J. K., Petters, M. D., Kreidenweis, S. M., Qafoku, O., Laskin, A., Roberts, G. C., and Prather, K. A.: Impact of Particle Generation Method on the Apparent Hygroscopicity of Insoluble Mineral Particles, Aerosol Sci. Technol., 44, 830-846, 10.1080/02786826.2010.497514, 2010.

Takegawa, N., Miyakawa, T., Kawamura, K., and Kondo, Y.: Contribution of selected dicarboxylic and omega-oxocarboxylic acids in ambient aerosol to the m/z 44 signal of an aerodyne aerosol mass spectrometer, Aerosol Sci. Technol., 41, 418-437, 10.1080/02786820701203215, 2007.

Tang, M. J., Cziczo, D. J., and Grassian, V. H.: Interactions of Water with Mineral Dust Aerosol: Water Adsorption, Hygroscopicity, Cloud Condensation, and Ice Nucleation, Chemical Reviews, 116, 4205-4259, 10.1021/acs.chemrev.5b00529, 2016.

Tang, M. J., Whitehead, J., Davidson, N. M., Pope, F. D., Alfarra, M. R., McFiggans, G., and Kalberer, M.: Cloud condensation nucleation activities of calcium carbonate and its atmospheric ageing products, Phys. Chem. Chem. Phys., 17, 32194-32203, 10.1039/c5cp03795f, 2015.

Varga, Z., Kiss, G., and Hansson, H. C.: Modelling the cloud condensation nucleus activity of organic acids on the basis of surface tension and osmolality measurements, Atmos. Chem. Phys., 7, 4601-4611, 10.5194/acp-7-4601-2007, 2007.

Yamashita, K., Murakami, M., Hashimoto, A., and Tajiri, T.: CCN Ability of Asian Mineral Dust Particles and Their Effects on Cloud Droplet Formation, Journal of the Meteorological Society of Japan, 89, 581-587, 10.2151/jmsj.2011-512, 2011.

Zhao, D. F., Buchholz, A., Mentel, T. F., Muller, K. P., Borchardt, J., Kiendler-Scharr, A., Spindler, C., Tillmann, R., Trimborn, A., Zhu, T., and Wahner, A.: Novel method of generation of $Ca(HCO_3)_2$ and $CaCO_3$ aerosols and first determination of hygroscopic and cloud condensation nuclei activation properties, Atmos. Chem. Phys., 10, 8601-8616, 10.5194/acp-10-8601-2010, 2010.

Zuend, A., Marcolli, C., Booth, A. M., Lienhard, D. M., Soonsin, V., Krieger, U. K., Topping, D. O., McFiggans, G., Peter, T., and Seinfeld, J. H.: New and extended parameterization of the thermodynamic model AIOMFAC: calculation of activity coefficients for organic-inorganic mixtures containing carboxyl, hydroxyl, carbonyl, ether, ester, alkenyl, alkyl, and aromatic functional groups, Atmospheric Chemistry and Physics, 11, 9155-9206,

897 10.5194/acp-11-9155-2011, 2011.

Table 1. Mode diameters, chemical compositions, and κ values of $CaCO_3$ aerosol particles (size selected by DMA at 101.8 nm) before (uncoated) and after coating with oleic (OA) or malonic acid (MA) at 30-80 ºC.

	D_P [nm]	Organic mass per particle [10^{-12}µg]	Mole organics per particle [10^{-20} mole]	Org. volume fraction [%]	κ
Oleic acid					
Uncoated $CaCO_3$ 30-80 ºC	101.9	(backgr. *m/z*41: 2.7±0.9)	0	0.0	0.0028±0.0001
$CaCO_3$+Oleic acid 30 ºC	102.1	3.7±1.9	1.3	0.8	
$CaCO_3$+Oleic acid 40 ºC	102.5	7.0±2.8	2.5	1.4	
$CaCO_3$+Oleic acid 50 ºC	103.7	14±3.7	5.1	2.7	
$CaCO_3$+Oleic acid 60 ºC	104.9	23±1.2	8.3	4.3	
$CaCO_3$+Oleic acid 70 ºC	109.2	96±3.7	34	16	0.0241±0.0006
$CaCO_3$+Oleic acid 80 ºC	123.7	390±14	140	44	0.0649±0.0008
Malonic acid					
Uncoated $CaCO_3$ 30-80 ºC	101.9	(backgr. *m/z*42: 1.4±0.4)	0	0.0	0.0028±0.0001
$CaCO_3$+Malonic acid 30 ºC	102.0	3.3±0.3	3.2	0.4	0.0123±0.0005
$CaCO_3$+Malonic acid 40 ºC	102.1	6.8±1.2	6.5	0.8	0.0231±0.0008
$CaCO_3$+Malonic acid 50 ºC	102.2	13±1.8	13	1.5	0.0380±0.0012
$CaCO_3$+Malonic acid 60 ºC	102.7	38±1.6	36	4.1	0.1063±0.0023
$CaCO_3$+Malonic acid 70 ºC	107.8	160±8.1	160	15	0.1907±0.0031
$CaCO_3$+Malonic acid 80 ºC	121.0	610±24	590	40	0.3126±0.0062

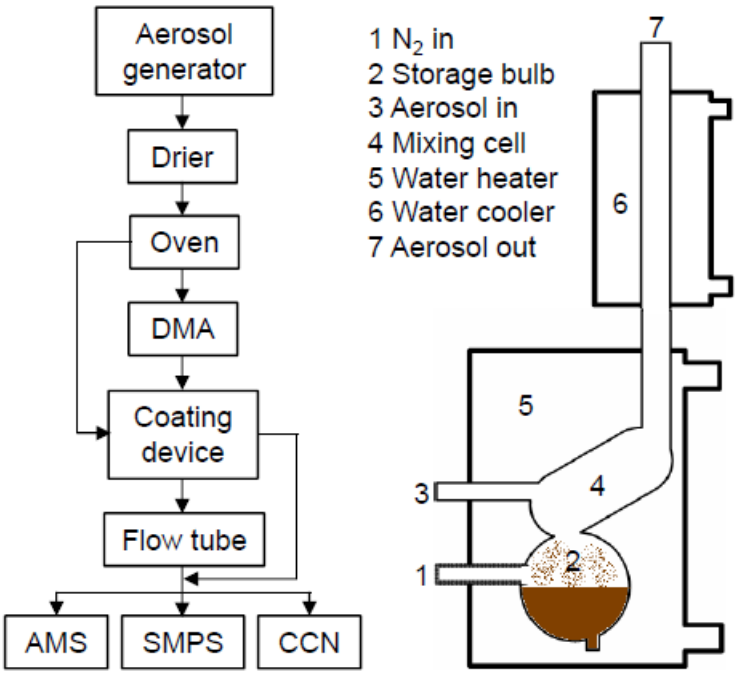

Figure 1. Schematics of the experimental set up (left side). $CaCO_3$ aerosol is generated by spray-drying of saturated $Ca(HCO_3)_2$ solutions and tempering the aerosol passing through an oven at 300 °C. The *poly-disperse* $CaCO_3$ aerosol is either led directly to the coating device (right side, after Roselli, 2006) or led to a differential mobility analyzer (DMA) for size selection first. Optional, a flow tube can be switched into the pass to enhance the reaction time of the coated particles. The stream of coated particles is finally split to the analytical instruments, namely aerosol mass spectrometer (AMS), scanning mobility particle sizer (SMPS) and CCN counter.

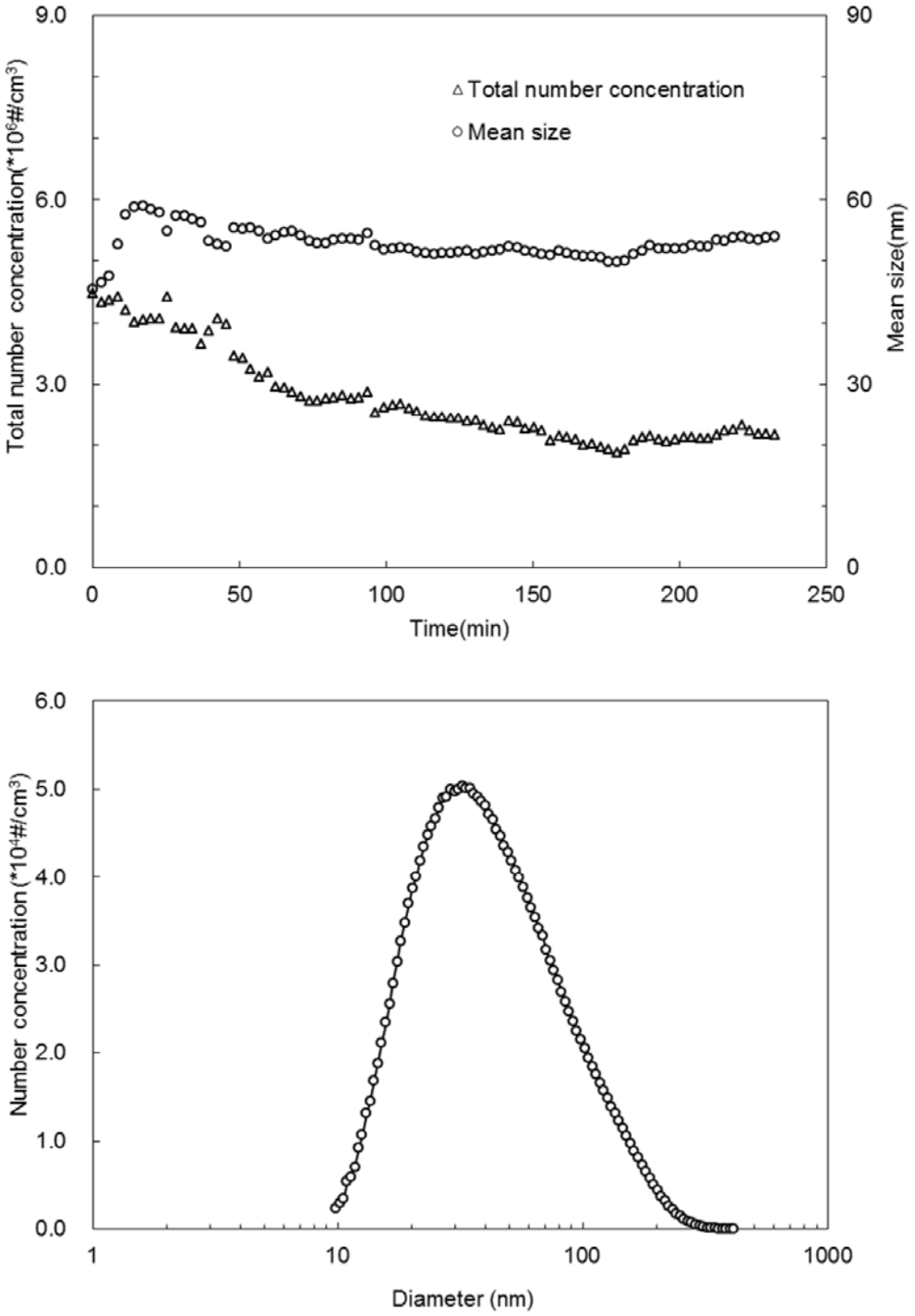

Figure 2. Total number concentration and mean diameter of $CaCO_3$ aerosol particles generated as a function of the spraying time (upper panel). Typical size distribution of the $CaCO_3$ aerosol after 70 min spraying (lower panel).

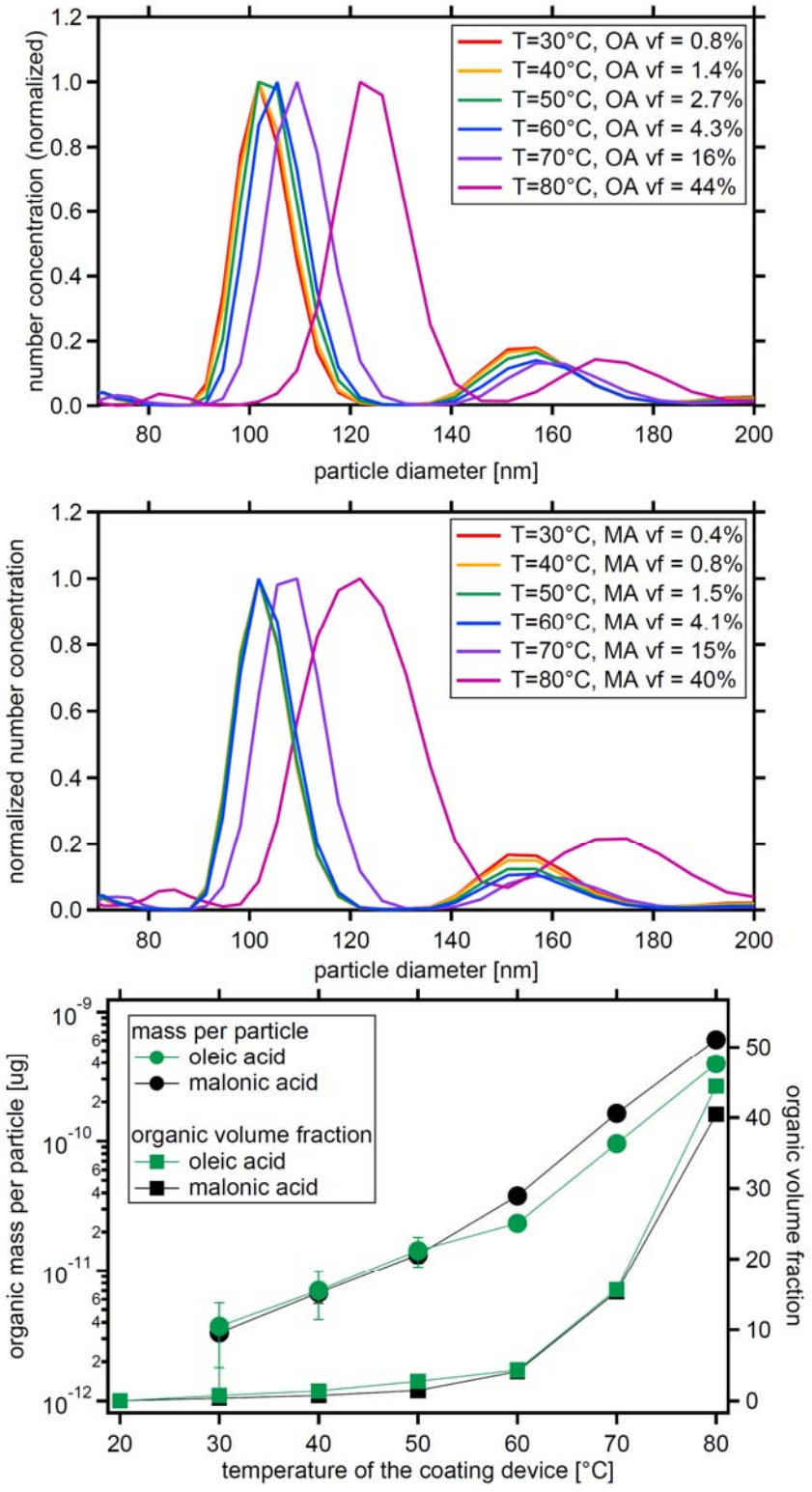

Figure 3. Size distribution of monodisperse $CaCO_3$ aerosol particles after coating with oleic acid (top panel) or malonic acid (middle panel). Coating amount and organic volume fraction for oleic and malonic acid as a function of the coating temperature for the same experiments (bottom panel, data in Table 1).

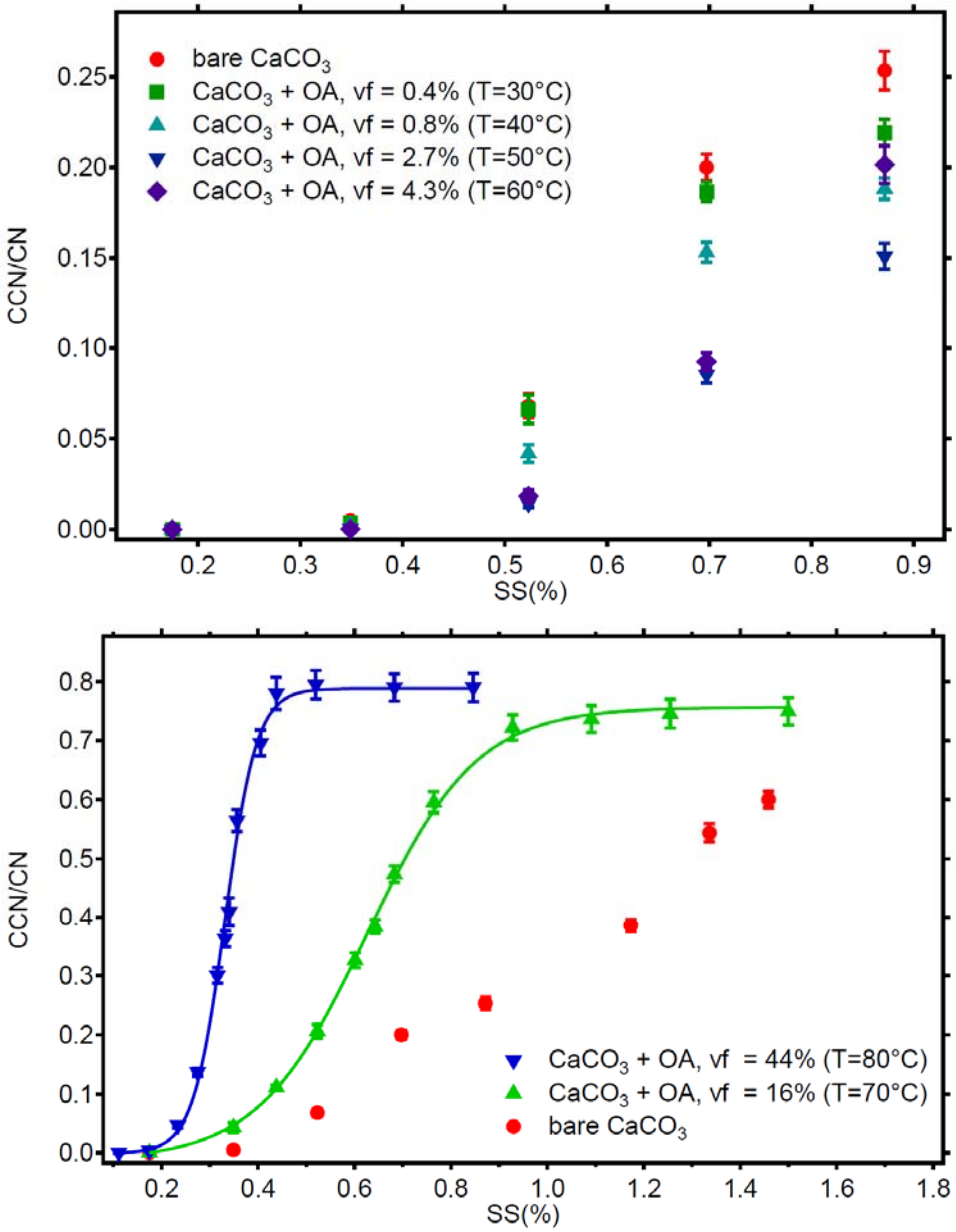

Figure 4. Activated fractions (CCN/CN) of *monodisperse* $CaCO_3$ aerosol particles (diameter d_u = 101.9 nm) at different supersaturations before and after oleic acid coating. With increasing coating temperatures of 30-50 ºC the activated fraction decreases despite the increase of organic vf from 0.8% - 2.7%. At vf = 4.3% at 60 °C this trend turns. Considering the increased particle diameter at 30-60 ºC and the reduced activated fraction simultaneously, the CCN activity of the coated $CaCO_3$ particles at 30-60 ºC was lower than that of the uncoated $CaCO_3$ particles (top panel). At coating vf of 16% and 44% (T= 70-80 ºC) the activated fractions, thus CCN activities, are higher than for bare $CaCO_3$ and increase with coating vf. In these two cases all particles are activated at the highest SS and SS_{crit} and κ can be determined from the turning point of the sigmoidal fit (bottom panel, compare Table 1).

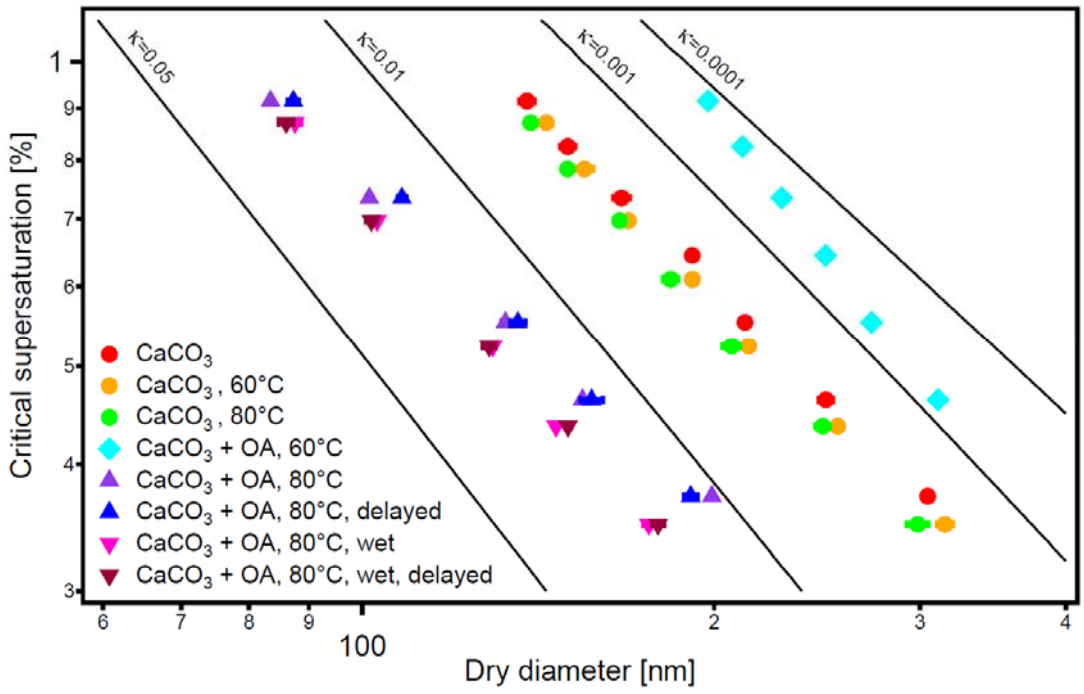

Figure 5. Critical dry diameters at different supersaturations (SS) of *poly-disperse* $CaCO_3$ aerosol before (circles) and after oleic acid coating. Experiments were performed at 60°C (turquoise diamond) and 80°C (triangles) coating temperatures. The flow tube experiments at 80° C were performed (indicated by 'delayed') at dry conditions (normal, blue tringles) and at enhanced water vapor ('wet', brown triangles). The effect of the temperature in the coating device on the $CaCO_3$ core is negligible (red, green, and orange circles). As for the monodisperse case in Figure 4, at 60° coating temperature the particles are less CCN active than bare $CaCO_3$ while at 80°C the coated particle more CCN active. The presence of water vapor (1500 Pa) in the coating process enhances CCN activity. The increasing of residence time (23.7 s) of the coated aerosol in the flow tube had no significant effect on CCN activity in both experiments.

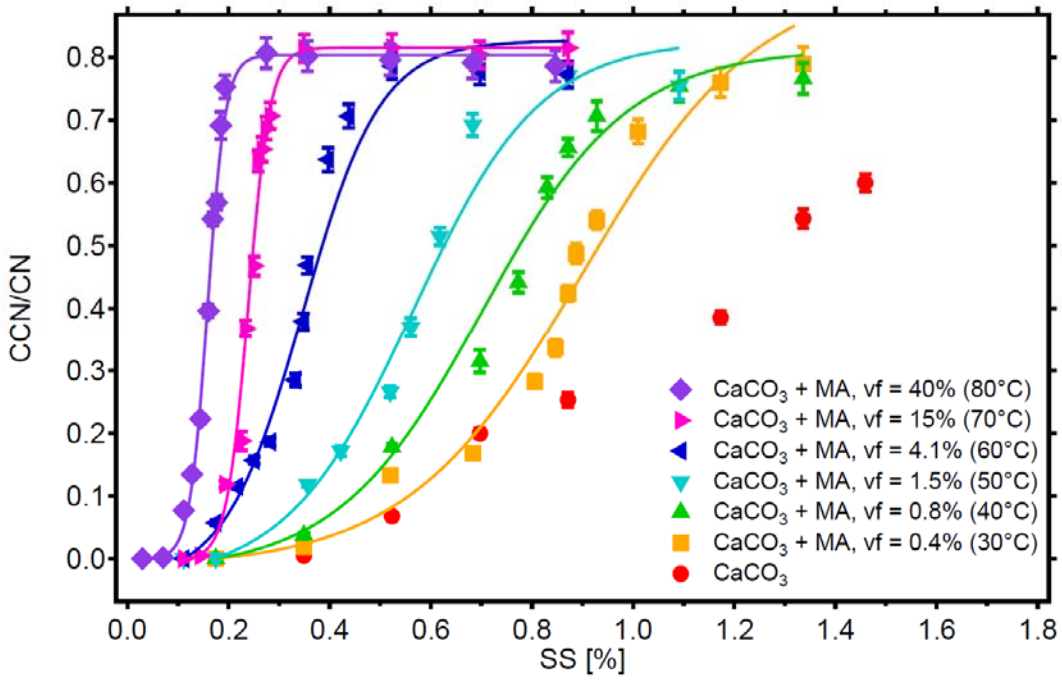

Figure 6. Activated fractions (CCN/CN) of *monodisperse* $CaCO_3$ aerosol particles (with $CaCO_3$ core, d_u = 101.9 nm) at different supersaturations before (red circles) and after malonic acid coating. With increasing coating, i.e. MA volume fraction vf the activated fraction, thus CCN activity, increase compared to bare $CaCO_3$ particles. All coated particles can be activated at sufficiently high SS and SS_{crit} and κ was determined (see Table 1).

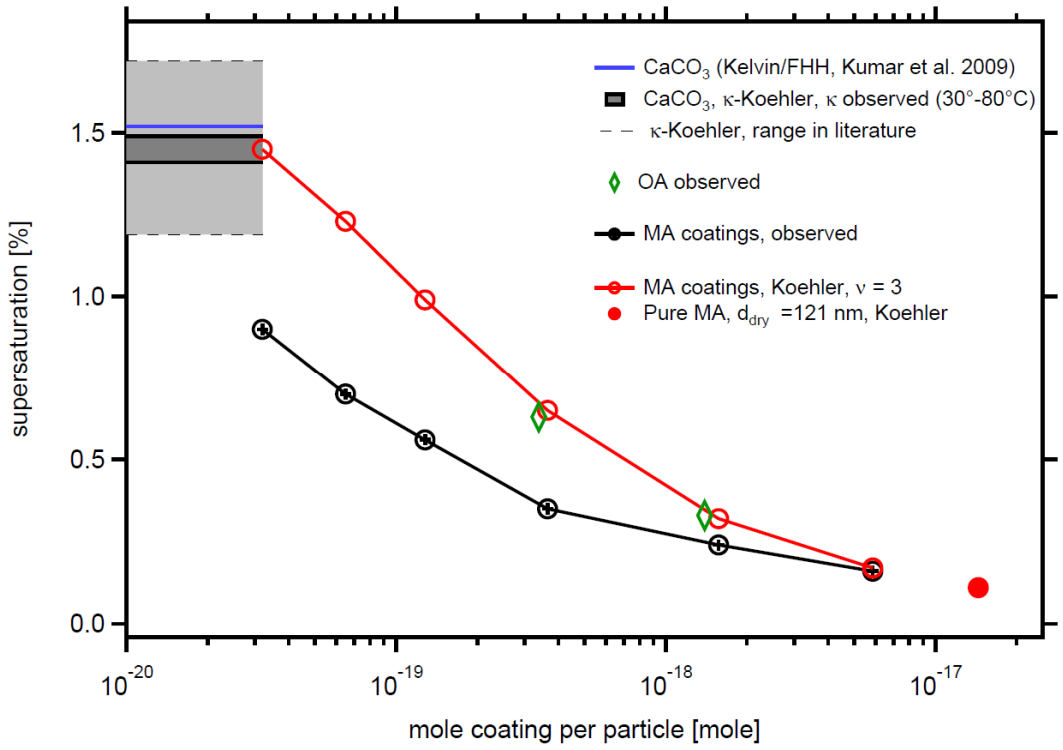

Figure 7. Comparison of SS_{crit} predicted by Koehler theory with observations. Koehler theory for aqueous MA solutions assuming full dissociation (ν=3) overpredicts SS_{crit} (red circles) compared to the observation (black circles). With increasing coating amount Koehler theory approaches the observation, with the limiting SS_{crit} for 121.0 nm particles made of pure malonic acid. For comparison we show also observed SS_{crit} for the two thickest OA coatings (green diamonds). The horizontal lines indicate SS_{crit} of the bare $CaCO_3$ particles as calculated from our observed κ (black) and predicted by Kelvin/FFH theory (blue). Light grey area between the thin dashed grey lines shows the range of SS_{crit} for 101.9 nm particles calculated from the range of κ in literature for wet generated $CaCO_3$ particles (compare Tang et al. 2016).

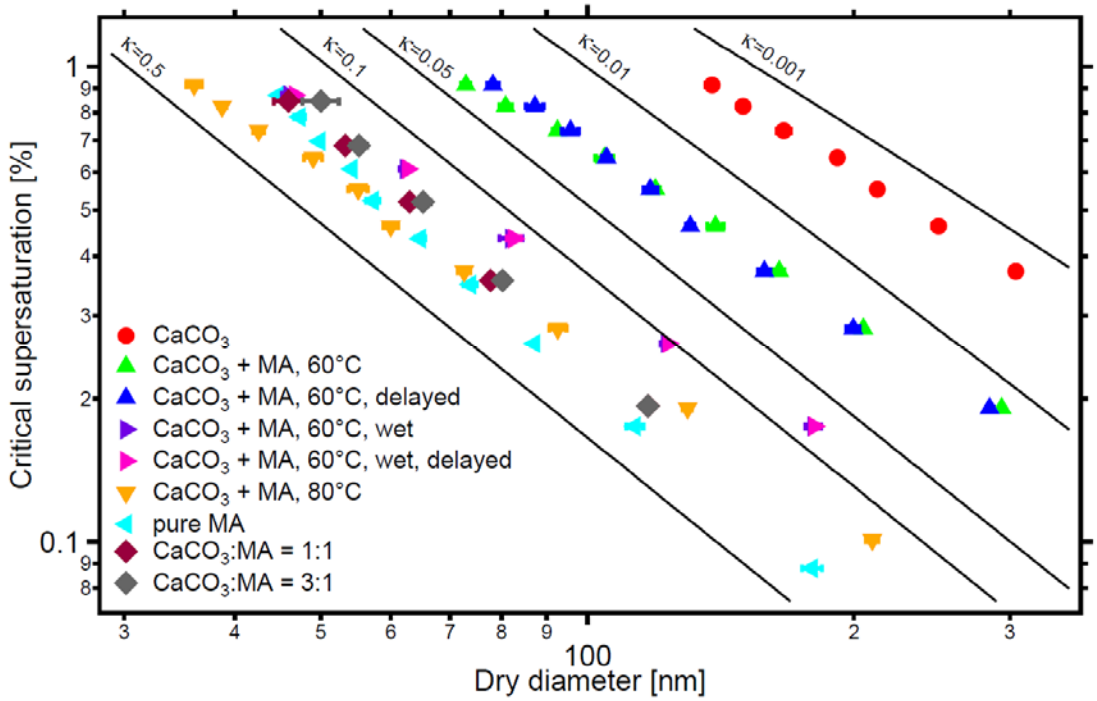

Figure 8. Critical dry diameters at different supersaturations (SS) of *poly-disperse* $CaCO_3$ aerosol before (circles) and after malonic acid coating (triangles). Experiments were performed at 60°C and 80°C coating temperatures. The results are similar to the monodisperse case in Figure 6. Critical dry diameters as a function of SS are also shown for malonic acid particles and particles that were generated by spraying mixed solution with molar ratios of $CaCO_3$/malonic acid of 1:1 and 3:1. The CCN activity decreases with increasing $CaCO_3$ content. The flow tube experiments at 60 °C were performed (indicated by 'delayed') at dry condition (blue tringles) and in presence of 1500 Pa water vapor (magenta triangles). The presence of water in the coating process substantially enhanced κ and CCN activity. The increasing of residence time (23.7 s) of the coated aerosol in the flow tube had no significant effect on CCN activity in both experiments.